

Dalton Transactions

An international journal of inorganic chemistry

Accepted Manuscript

This article can be cited before page numbers have been issued, to do this please use: J. Geßner, S. G. Ebbinghaus and J. Jacobs, *Dalton Trans.*, 2025, DOI: 10.1039/D5DT01138H.



This is an Accepted Manuscript, which has been through the Royal Society of Chemistry peer review process and has been accepted for publication.

Accepted Manuscripts are published online shortly after acceptance, before technical editing, formatting and proof reading. Using this free service, authors can make their results available to the community, in citable form, before we publish the edited article. We will replace this Accepted Manuscript with the edited and formatted Advance Article as soon as it is available.

You can find more information about Accepted Manuscripts in the [Information for Authors](#).

Please note that technical editing may introduce minor changes to the text and/or graphics, which may alter content. The journal's standard [Terms & Conditions](#) and the [Ethical guidelines](#) still apply. In no event shall the Royal Society of Chemistry be held responsible for any errors or omissions in this Accepted Manuscript or any consequences arising from the use of any information it contains.

Structure, Magnetism and Thermal Stability of the

View Article Online
DOI: 10.1039/C5DT01138H

$n = 3$ Ruddlesden-Popper Oxyfluoride



*Jakob Geßner¹, Stefan G. Ebbinghaus¹ and Jonas Jacobs^{1, *}*

¹ Martin Luther University Halle-Wittenberg, Faculty of Natural Sciences II, Institute of Chemistry,
Inorganic Chemistry, Kurt-Mothes-Straße 2, 06120, Halle, Germany



ABSTRACTView Article Online
DOI: 10.1039/D5DT01138H

Oxides of the Ruddlesden-Popper (RP) series $A_{n+1}B_nO_{3n+1}$ are ideal candidates for the incorporation of additional anions like F^- , H^- , or N^{3-} in the crystal lattice. The resulting mixed anionic compounds usually exhibit clearly different physical properties compared to the precursor oxides due to changes in their atomic and electronic structure. We present the synthesis of the highly fluorinated $n = 3$ oxyfluoride $La_4Ni_3O_{8.4}F_{3.5}$ by topochemical fluorination of $La_4Ni_3O_{10}$, with poly(vinylidene difluoride) (PVDF) as fluoride source. The structure of this compound is solved based on X-ray and neutron powder diffraction data. A monoclinic ($P2_1/a$, $a = 5.4206(2)$ Å, $b = 5.5081(2)$ Å, $c = 29.9823(2)$ Å, and $\beta = 90.85(1)^\circ$) distorted variant of the $n = 3$ RP structure was found showing a strong elongation perpendicular to the perovskite slabs resulting from full occupation of the interstitial anion positions. The formation reaction as well as the decomposition reaction was investigated by *in situ* X-ray diffraction. By this the presence of one distinct formation intermediate was revealed. The thermal decomposition was found to start 490°C and is accompanied by the release of oxygen as detected by coupled mass spectrometry. Temperature and field depended magnetization measurements indicate that the title oxyfluoride is a Curie-Weiss paramagnet in contrast to the parent oxide, which shows Pauli paramagnetism highlighting the strong impact of anion substitution on the physical properties of these mixed anionic compounds.



Introduction

View Article Online
DOI: 10.1039/D5DT01138H

The crystal structure of Ruddlesden-Popper (RP) oxides can be described as alternating stacks of n perovskite layers ABO_3 and one single rock salt layer AO . This stacking results in the general formula $A_{n+1}B_nO_{3n+1}$ where $n = 1, 2, 3$ or even higher.^{1,2} Here A often is a lanthanide or alkaline earth ion and B in most cases is a transition metal cation.³

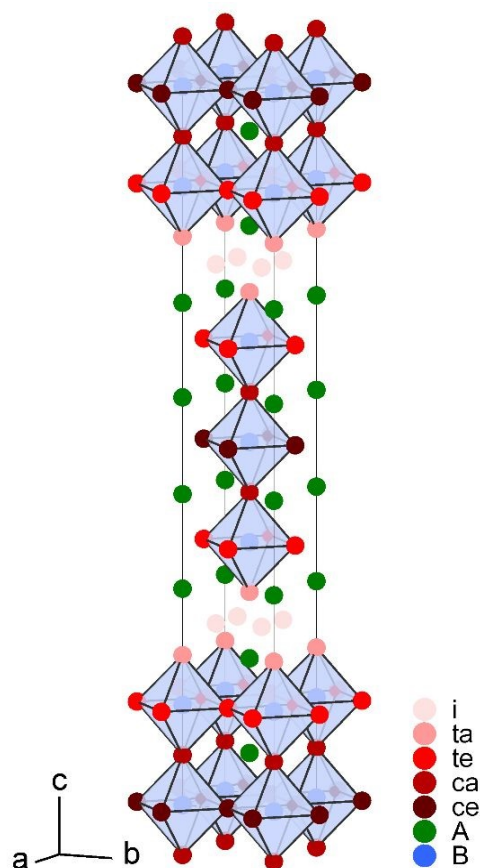


Figure 1: Representation of the ideal $n = 3$ Ruddlesden-Popper structure (space group $I4/mmm$). The BO_6 octahedra are shown and the different anion sites are indicated by different shades of red.

Mixed anion Ruddlesden-Popper oxides often exhibit interesting physical properties such as gap values in the range of the solar spectrum,^{4,5} ferroelectricity,⁵⁻⁷ ionic transport,^{8,9} or altermagnetism.^{10,11} There are even examples showing high-temperature superconductivity.^{12,13} In the highest symmetric version of the $n = 3$ RP structure (space group: $I4/mmm$, (Figure 1)) four different anionic sites exist, which form the vertices of the BO_6 octahedra of the perovskite slab: central apical (ca , $4e$, $(0,0,z_1)$), central equatorial (ce , $4c$, $(1/2,0,0)$), terminal apical (ta , $4e$, $(0,0,z_2)$) and terminal equatorial (te , $8g$, $(1/2,0,z_3)$). In addition, a fifth anion site is located



within the rock salt layer (*i*, $8f$, ($\frac{1}{4}$, $\frac{1}{4}$, $\frac{1}{4}$)), which is usually unoccupied but can take up to two additional anions per formula unit.

Other ions, such as nitride,^{4,5} hydride,^{14,15} hydroxide,^{16,17} halide^{3,8,18–21} or even carbonate²² ions can be located on this interstitial sites, resulting in mixed anionic materials with different properties compared to the corresponding oxides. This additive insertion of anions in the rock salt-type layer often results in an increase of the average oxidation number of the cations. The formation of such mixed anionic compounds can additionally occur from partial substitution of O^{2-} ions, where in the case of O^{2-}/F^- a substitution on the apical sites is often found as favored over a statistical distribution to the apical and equatorial sites.²³

For the more comprehensively investigated group of $n = 1$ RP oxyfluorides, there are examples of both anion substitution scenarios: In K_2NbO_3F the fluoride ions occupy the apical vertices in a disordered manner^{24,25}, whereas in Sr_2FeO_3F the apical sites are occupied in an ordered way. Due to the increased Fe–F bond length compared to the Fe–O bonds, this substitution leads to square-pyramidal coordination of the Fe^{3+} ions.^{21,26} Examples for the insertion of F^- into the interstitial sites are $La_2CoO_4F_{1.2}$ with unordered occupation,²⁷ $LaSrMnO_4F$ with layer-wise ordering of fluoride-occupied and empty interstitial sites²⁸ and $Ba_{2-x}Sr_xPdO_2F_2$, where the interstitial sites are fully occupied, resulting in a square-planar coordination of Pd^{2+} .²⁹ Finally, there are compounds where both anion sites, apical and interstitial, are occupied by fluoride, e.g. $La_2NiO_{2.5}F_3$,¹⁹ or $Sr_2TiO_3F_2$.³⁰ To our knowledge, there are no $n = 1$ RP oxyfluorides where the equatorial sites are solely occupied by F^- .

For the $n = 2$ RP oxyfluorides there are also reports for a variety of anion ordering scenarios with examples for F^- occupying only interstitial sites,^{31,32} only terminal apical sites^{33,34}, or both, interstitial and terminal apical sites as in $La_3Ni_2O_{5.5}F_{3.5}$ ³⁵ or other related compounds.^{36,37} As with the $n = 1$ case, there are no studies indicating occupancy of the equatorial vertices of the octahedrons by F^- . Furthermore, to the best of our knowledge, no fluoride occupation of central apical anion sites has been reported, either.



Only very few $n = 3$ RP oxyfluorides are known so far. The four compounds $\text{La}_{0.5}\text{Sr}_{3.5}\text{Fe}_3\text{O}_{7.5}\text{F}_{2.6}^3$, $\text{La}_4\text{Co}_3\text{O}_{10}\text{F}_2^{38}$, $\text{La}_4\text{Ni}_3\text{O}_8\text{F}_{0.84}^{39}$ and $\text{La}_4\text{Ni}_3\text{O}_8\text{F}_{1.7}^{39}$ are the only members described in literature to date. For all compounds an increase in the unit cell parameter c was found, compared to the parent oxides. With Δc in the region of ~ 3 Å a clear sign of a full interlayer occupation was found for $\text{La}_4\text{Co}_3\text{O}_{10}\text{F}_2$ while for $\text{La}_{0.5}\text{Sr}_{3.5}\text{Fe}_3\text{O}_{7.5}\text{F}_2$ with $\Delta c \sim 1.2$ Å only a partially interlayer occupation in combination with a fully terminal apical occupation was derived from refinement of neutron powder diffraction data. The nickel compounds $\text{La}_4\text{Ni}_3\text{O}_8\text{F}_{0.84}$, $\text{La}_4\text{Ni}_3\text{O}_8\text{F}_{1.7}$ were obtained from fluorination of the reduced RP-oxide $\text{La}_4\text{Ni}_3\text{O}_8$ with XeF_2 . A partial O/F ordering and the presence of highly elongated NiO_4F_2 octahedra were derived based on X-ray diffraction data. The elongated octahedra were seen as indication for an occupation of the terminal apical anion sites by F^- .

Different methods are applied to obtain such oxyfluoride. The fluorination applied here, follows the low-temperature route first described by Slater.⁴⁰ The use of fluorinated organic polymers such as poly(vinylidene difluoride) (PVDF; $(\text{CH}_2\text{F}_2)_n$) often yields oxyfluorides of higher quality than other fluorinating agents such as NH_4F , CuF_2 , or F_2 -gas, which are sometimes difficult to handle and whose products tend to remain as impurities in the obtained samples.^{41–45} The PVDF-based fluorination method was also applied to obtain the above-mentioned $n = 3$ compounds $\text{La}_{0.5}\text{Sr}_{3.5}\text{Fe}_3\text{O}_{7.5}\text{F}_{2.6}^3$, $\text{La}_4\text{Co}_3\text{O}_{10}\text{F}_2^{38}$ as well as the $n = 1$ nickelate oxyfluorides $\text{La}_2\text{NiO}_3\text{F}_2^{46,47}$ and $\text{La}_2\text{NiO}_{2.5}\text{F}_3$.¹⁹

In this study, we present the successful synthesis of the $n = 3$ RP oxyfluoride with the formula $\text{La}_4\text{Ni}_3\text{O}_{8.4}\text{F}_{3.5}$, which was synthesized by topochemical fluorination of $\text{La}_4\text{Ni}_3\text{O}_{10}$, obtained from citrate synthesis, with PVDF as fluorine source. The oxyfluoride crystallizes in the monoclinic space group $P2_1/a$. Its structure was solved by Rietveld refinement based on neutron and X-ray powder diffraction (XRD) data in combination with elemental analysis methods (e.g. XRF, iodometric titration, F^- determination by ISE). *In situ* XRD experiments were used to trace the formation reaction and the thermal decomposition reaction of the oxyfluoride. Here,



the presence of reaction intermediates, one for the formation and one for the decomposition, each with different crystal structure was revealed. The observation of the decomposition intermediate is accompanied by the release of oxygen as identified via mass spectrometry. The temperature and field dependent magnetic behavior was also investigated and a change from a Pauli paramagnetism of the precursor oxide to Curie-Weiss paramagnetism is found for $\text{La}_4\text{Ni}_3\text{O}_{8.4}\text{F}_{3.5}$.

Experimental Section

Synthesis

The synthesis of $\text{La}_4\text{Ni}_3\text{O}_{8.4}\text{F}_{3.5}$ was done in a two-step procedure. First, the precursor oxide $\text{La}_4\text{Ni}_3\text{O}_{10}$ was synthesized by a citric acid complexation method. Stoichiometric amounts of La_2O_3 (Chempur, 99.99%; dried at 900 °C for 3 h) and Ni powder (VEB-Jenapharm, 99.5%) were dissolved in demineralized water under the dropwise addition of concentrated HNO_3 . Citric acid (Grüssing) was added in a molar ratio of 3:1 to the metal cations while stirring. Water was evaporated from the solution on a hot plate until a gel-like substance was obtained. Further heating of this gel at 350 °C resulted in self ignition. The resulting material was further heated in a box furnace at 450 °C for 6 h to decompose the remaining organic compounds. The resulting blackish powder was then ground in an agate mortar and calcined at 1000 °C for 24 h. Fluorination was performed by mixing the precursor oxide with PVDF (Alfa Aesar) in a 1:2 ratio according to the mass of its monomeric unit CH_2CF_2 . The mixture was heated in air at 370 °C for 16 h and allowed to cool down to room temperature, yielding in the final oxyfluoride.

Characterization

Room temperature powder X-ray diffraction (XRD) patterns in the range $2\theta = 10\text{--}140^\circ$ with a step size of 0.01° and a time of 3 s per step were recorded with $\text{Cu-K}_{\alpha 1,2}$ radiation on a Bragg–Brentano Bruker AXS D8 Advance diffractometer equipped with a LYNXEYE silicon strip



detector. In addition, a STOE STADI MP diffractometer with transmission geometry and monochromatic Mo-K_{α1} radiation equipped with a DECTRIS MYTHEN 1K detector was also used for room temperature scans in the angular range of $2\theta = 5-85^\circ$.

The latter diffractometer was also used to collect high temperature XRD data with a STOE capillary furnace. These patterns were recorded in the range $2\theta = 8-44^\circ$. To follow the formation reaction of the oxyfluoride, the sample was heated up to 370 °C and diffraction patterns were recorded every 7 minutes. To study the decomposition processes of the oxyfluoride in oxidative and reductive atmospheres (N₂, air, O₂), heating was performed at 50 K/min up to 250 °C, then at 10 K/min in the range of 250-650 °C and at 25 K/min from 650-900 °C. After each heating segment, a XRD scan with an acquisition time of ~10 min was performed. The transfer capillary of a mass spectrometer (Pfeiffer Vacuum OmniStar GSD 350), was inserted in the sample capillary using a self-made setup (compare Figure S 1) allowing for the analysis of the gaseous reaction products.

Neutron diffraction (ND) data of La₄Ni₃O_{8.4}F_{3.5} was collected on the high-resolution powder diffractometer D2B at the Institute Laue-Langevin in Grenoble, France. Beamtime was granted for Proposal 5-23-769⁴⁸ and measurement of the 1.1 g sample (in a 6 mm V-cylinder) was performed at 300 K with $\lambda = 1.594 \text{ \AA}$ and an acquisition time of about 3h.

Joint Rietveld refinements of XRD and ND data were performed using GSAS-II software.⁴⁹ Instrumental resolution parameters for the Bruker D8-Advance diffractometer were determined from the refinement of an α -Al₂O₃ reference scan. LaB₆ was used as reference material to determine the instrumental resolution parameters for the STOE STADI MP diffractometer.

Magnetic measurements were carried out using the ACMS option of a Quantum Design PPMS-9. Approximately 100 mg of the powder samples (oxide and oxyfluoride) were loaded in gelatin capsules, which were then attached to the end of a plastic straw. The gelatin capsules ensure a low diamagnetic contribution to the measured susceptibilities. The temperature dependent moment was measured at an external field of 0.1 T and 5 T in the temperature range of 5–300



K. For $B = 0.1$ T zero-field-cooled (ZFC) and field-cooled (FC) conditions were applied. The data for the measurement in $B = 5$ T was collected while warming of the previously field-cooled sample (FCW). The field dependence of the magnetic behavior was analyzed by recording the complete hysteresis from -5 to 5 T at 5 K.

The oxygen content of both, the oxide and the oxyfluoride was determined by thermogravimetric analysis (TGA) using a TA Instruments TGA550 thermo balance in flowing forming gas (furnace gas: 10% H_2 in N_2 , 25 mL/min; balance protecting gas: N_2 25 mL/min). The samples were heated to 950 °C at 10 K/min and held at this temperature for 10 min ensuring a full reduction.

The fluorination product was checked for residual PVDF as well as other carbon related impurities by infrared (IR) spectroscopy (Bruker Alpha) in the range of $\tilde{\nu} = 4000$ - 400 cm^{-1} .

The contents of La and Ni were quantified by X-ray fluorescence spectroscopy (XRF) (Panalytical Epsilon 4) using the standardless quantification mode (Omnian mode).

The average oxidation states of Ni in the precursor oxide and the oxyfluoride were determined by iodometric titration. Approximately 15 mg of the samples were dissolved in 5 M HCl containing an excess of KI. Afterwards ~ 1 g of Na_2CO_3 was added to provide a pseudo inert atmosphere of CO_2 . A 0.006 M $Na_2S_2O_3$ solution was used as titrant with starch solution as indicator. The oxidation state was averaged from three independent measurements per sample.

The amount of fluoride was quantified using a Mettler Toledo Seven Multi ion sensitive electrode (ISE). In a 100 mL PMP volumetric flask ~ 10 mg of the sample was dissolved in 10 mL of 5 M HCl. The dissolved cations were complexed with 10 mL of a Titriplex IV solution ($c = 6.82$ g/L). The pH value was adjusted to ~ 6 against bromothymol blue indicator by adding a CH_3COOH/CH_3COONa buffer and NaOH solution ($c = 5$ mol/L). The flask was then topped with demineralized water. The F^- content was obtained from five-point standard addition (40 mL sample solution, addition of 5×100 μL of a 1 g/L F^- standard solution (Mettler



Toledo) using a single channel pipette, for a total of six measurements per sample)³ The final F-content was averaged from three independent solutions per sample.

Scanning electron microscopy (SEM) was performed with a Phenom ProX desktop electron microscope. The powdered samples were spread onto carbon tape and images were collected in backscattered electron mode (BSE) with an acceleration voltage of 10 keV.

The analysis of the Ni oxidation state was carried out by X-ray photoelectron spectroscopy (XPS) using a DAR 400 instrument (Omicron) with an Al-K α line (1486 eV, 250 W) as X-ray source and an EA 125X Hemispherical Energy Analyzer (Omicron). Survey scans were performed with 100 eV pass energy, detail scans of the Ni3p region with a pass energy of 30 eV. The spectra were fitted and analyzed using the CasaXPS software.

Results & discussion

In previous investigations on the $n = 1$ oxyfluorides La₂NiO₃F₂ and La₂NiO_{2.5}F₃ we demonstrated that isothermal *in situ* X-ray powder diffraction can be used to obtain insight in the reaction intermediates occurring during the fluorination reaction as well as to obtain suitable parameters for bulk synthesis.⁵⁰ We also showed that the use of precursor oxides obtained from soft chemistry are beneficial for obtaining phase-pure oxyfluorides, most probably due to smaller particle sizes.^{19,47} This is why we started our investigations with *in situ* XRD experiments for the fluorination of La₄Ni₃O₁₀ obtained from citrate synthesis.

Structural and Compositional Characterization of La₄Ni₃O_{8.4}F_{3.5}

Different Oxide:PVDF ratios (1:1, 1:1.5, and 1:2) were initially tested and a single-phase product was obtained for the 1:2 ratio corresponding to a nominally 4 F⁻ per f.u.. The *in situ* XRD data obtained for the 1:2 reaction mixture at 370 °C is shown in Figure 2 and the diffraction patterns of the precursor oxide (bottom) and the reaction product (top) are additionally given. From the additional reflections found in the time range of 4 - 7 h in the



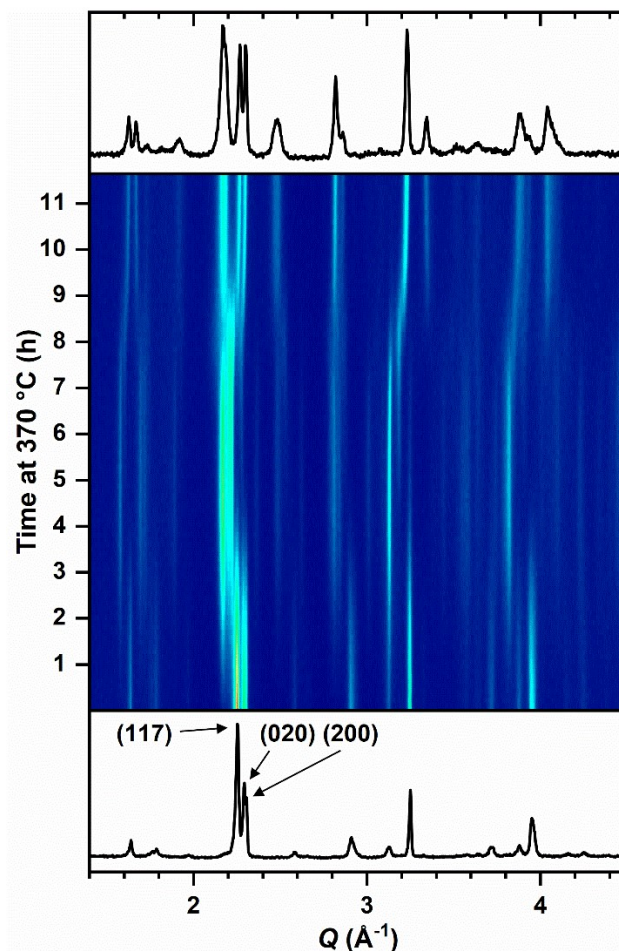


Figure 2: Time dependent *in situ* XRD patterns of the reaction of $\text{La}_4\text{Ni}_3\text{O}_{10}$ with PVDF (molar ratio 1:2) obtained at 370 °C. Bottom and top diffraction patterns are the initial and final pattern.

contour plot of Figure 2 it is apparent that the reaction to the final oxyfluoride proceeds via one reaction intermediate. This intermediate possesses a larger unit cell than the oxide, which is indicated by the significant shift of (117) as well as (200)/(020) (please note that all (hkl) values are given with respect to the orthorhombic $Fmmm$ coordinate system with c as longest axis) to smaller Q values. Upon longer heating, the formation of the final oxyfluoride is achieved. Here a clear shift of (200)/(020) to higher Q values indicate a decrease in the size of the basal ab -plane, which is accompanied by a further elongation of c as the most intense (117) signal shifts to even lower Q values. The observation of a distinct reaction intermediate is in contrast to the reaction of closely related compound $\text{La}_4\text{Co}_3\text{O}_{10}$ with PVDF, where the product $\text{La}_4\text{Co}_3\text{O}_{10}\text{F}_2$ is formed directly.³⁸ For the $n = 1$ nickelates, on the other hand, the presence of several reaction intermediates was previously found.⁵⁰ Efforts to isolate the intermediate of the fluorination



reaction through targeted synthesis as well as quenching remained unsuccessful. From quenching experiments, a range of samples was obtained, which appeared to be mixtures of the precursor oxide and the final fluorination product. To extract the unit cell parameters of the intermediate *Le Bail* fits to the *in situ* XRD data were performed in space group *Fmmm*. The following unit dimensions were obtained for the 370°C data $a = 5.662 \text{ \AA}$, $b = 5.705 \text{ \AA}$, and $c = 29.223 \text{ \AA}$. Full structure refinements were not attempted as the present data quality is not sufficient enough. Nonetheless, the detailed investigation of the formation reaction is planned for a future publication.

Bulk synthesis of the oxyfluoride was performed with oxide:PVDF mixtures (1:2 ratio) at 370 °C for 16 h. This results in the highly fluorinated black product $\text{La}_4\text{Ni}_3\text{O}_{8.4}\text{F}_{3.5}$. SEM investigations give irregular shaped particles with diameters of 0.5-1 μm (see Figure S 2). The morphology of these particles does not differ significantly from the particles of the starting oxide. IR spectra (see Figure S 3) show high absorption in the entire range 4000 to 400 cm^{-1} but no signals of PVDF indicating the absence of residual PVDF or other carbon related impurities in the resulting product. The fluoride content of the oxyfluoride was determined using a fluoride ion sensitive electrode by applying the standard addition technique. The obtained value of 7.15(4) % corresponds to 3.5(2) F^- per formula unit, which is clearly less than the nominal 4 F^- per f.u. expected from the amount of PVDF used. This deviation reveals that not all fluorine from the PVDF is incorporated into the oxide lattice. A similar finding was observed in the synthesis of $\text{La}_{0.5}\text{Sr}_{3.5}\text{Fe}_3\text{O}_{7.5}\text{F}_{2.6}$ where 3 F^- per f.u. are expected from the amount of PVDF used. Based on these findings, synthesis experiments with an extended range of oxide:PVDF ratios were performed in finer steps (see diffraction patterns in Figure S 4) were carried out. It was found that the 1:1.75 oxide:PVDF ratio (nominally 3.5 F^- per f.u.) also result in a phase-pure product but with slightly decreased lattice parameters. This points to a rather wide accessibility range of the oxyfluoride. The structural investigations of the here presented



work (*vide infra*) were nevertheless performed for the 1:2 product hence neutron diffraction data was obtained for this compound. Assuming La^{3+} and taking into account the result of the XRF measurement ($\text{La} / \text{Ni} = 1.31$; which is in good agreement to the nominal molar ratio of 1.33), in combination with the results of the iodometric titration, it can be concluded that Ni has an average oxidation state of 2.76(11) in the oxyfluoride, which is comparable to the obtained average oxidation state of Ni in the precursor oxide of 2.68(4). According to this value and with 3.5 fluoride ions per f.u., the oxyfluoride should contain $\sim 8.4 \text{ O}^{2-}$ per f.u. for charge neutrality. XPS spectra were obtained for the oxide and the oxyfluoride. This enables a comparison of the surface oxidation state of nickel in both samples. Due to a heavy overlap of the Ni $2p_{3/2}$ and the La $3d_{3/2}$ peaks,^{19,46,51,52} the less well resolved Ni 3p peak was investigated. The corresponding spectra are given in Figure S 5 in the SI. The observed signal can be interpreted as overlap of the Ni^{2+} signal at $\sim 67.0 \text{ eV}$ and Ni^{3+} signal at 70.7 eV .⁵³ Upon fluorination a decrease of the Ni^{2+} signal is observed pointing to less Ni^{2+} species at the sample surface which is in concordance with the slight increase of the Ni oxidation state as found in the iodometric titration. In order to verify the oxygen content, thermogravimetric analysis in reducing atmosphere (50mL/min of 5% H_2 in N_2) was performed (see Figure S 6). It was found that nickel is reduced to its metallic state under the applied conditions, which was verified by a field dependent magnetization measurement at 300 K showing ferromagnetic behavior (see Figure S 7). On the other hand, in the XRD pattern of the reduction product (see Figure S 8), only LaOF could be identified, implying that nickel is amorphous. This decomposition reaction was also investigated by *in situ* XRD (*vide infra*). Given these products and the observed weight loss of 7.45 % during the reduction process, an initial oxygen stoichiometry of 8.4 is confirmed in good agreement with the expectation. Therefore, the sum formula $\text{La}_4\text{Ni}_3\text{O}_{8.4}\text{F}_{3.5}$ can be deduced for the title compound. The presence of ~ 12 anions per formula unit demands for fully

View Article Online
DOI: 10.1039/D5DT01138H



occupied interstitial anion positions, which is in agreement with the results from refinement of neutron powder diffraction data (*vide infra*).

Laboratory X-ray diffraction patterns of oxyfluoride samples from different batches are shown in Figure 3. Based on this data a significant anisotropic broadening of selected reflections (like (117)/(11-7)) is evident. This broadening is similar for all batches and is also found in the diffraction pattern presented by C. K. Blakely et al. for a compound denoted $\text{La}_4\text{Ni}_3\text{O}_8\text{F}_2$, which was obtained from fluorination of $\text{La}_4\text{Ni}_3\text{O}_8$ with XeF_2 as fluorination agent.³⁹ The authors indexed their diffraction pattern with an orthorhombic unit cell even though the same splitting of (117)/(11-7) is clearly visible in their data. This anisotropic reflection broadening is most likely the result of stacking faults in the perovskite like layer i.e. the random appearance of perovskite slabs with deviating layer thickness n . Such stacking faults are common for Ruddlesden popper compounds and result in in the observed broadening of all (hkl) reflections with $l \neq 0$.⁵⁴⁻⁵⁷ Clearly the anisotropic broadening is interfering the structure determination from laboratory X-ray diffraction data alone, which is why we performed different post synthetic

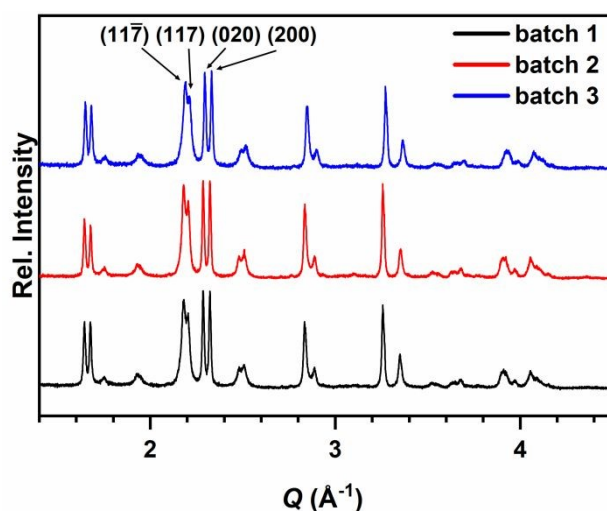


Figure 3: XRD patterns of $\text{La}_4\text{Ni}_3\text{O}_{8.4}\text{F}_{3.5}$ from different batches. The indices are given for the (117)/(11-7) and (200)/(020) reflexes indicating the difference in reflection broadening.

annealing experiments aiming to reduce the peak broadening. For the $n = 2$ compound $\text{La}_3\text{Ni}_2\text{O}_{5.5}\text{F}_{3.5}$ an improvement of the crystallinity upon heating in evacuated silica ampules was reported but unfortunately no X-ray diffraction patterns are shown of the crude or the



annealed product, which would allow for a comparison to the reflection broadening observed here.³⁵ We annealed our oxyfluoride samples in evacuated glass ampules for 5 days at 350 °C but unfortunately none of the experiments resulted in significantly sharper peaks.

The structure refinement was performed as joint refinement combining laboratory XRD with neutron powder diffraction data. The above discussed splitting of (117)/(11-7) demands for a monoclinic unit cell symmetry and indexing of the XRD-data was possible in space groups $P2_1/a$ (the space group of the starting oxide; please note the non-standard setting with c as longest axis, enabling an easier comparison to the $I4/mmm$ archetype) and $A2/a$ (the space group recently reported for the closely related oxyfluoride $\text{La}_4\text{Co}_3\text{O}_{10}\text{F}_2$).³⁸ In a subsequent Le Bail fit of the NPD data in $A2/a$ some reflections occurred, which should be integrally extinct in an A -centered lattice. These reflections can be indexed as (123), (027), and (207) (see Figure S 9) and a primitive unit cell is thus derived for $\text{La}_4\text{Ni}_3\text{O}_{8.4}\text{F}_{3.5}$. The subsequent structure refinement was therefore performed in $P2_1/a$ with $Z = 4$ and $a = 5.4206(2) \text{ \AA}$, $b = 5.5081(2) \text{ \AA}$,



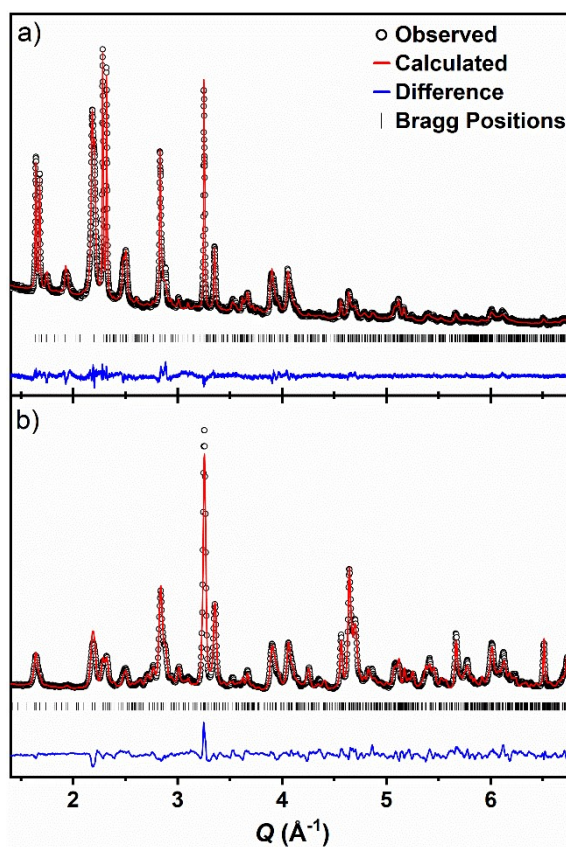


Figure 4: Rietveld plots of the joint refinements against a) X-ray ($\lambda = 1.542 \text{ \AA}$) and b) neutron diffraction data b) ($\lambda = 1.594 \text{ \AA}$) in space group $P2_1/a$.

$c = 29.9823(2) \text{ \AA}$, and $\beta = 90.85(1)$. The anisotropic peak broadening was taken into account by applying the Stephens model for general strain broadening.⁵⁸ To limit the number of refinable parameters the anisotropic strain parameters were constrained to be the same for both patterns (since the samples were from the same batch). Additionally, the thermal displacement parameters were constrained to be identical for the same type of atoms. The Rietveld plots obtained for the refinements in $P2_1/a$ are given in Figure 4 and the refined crystallographic parameters are listed in Table 1. Fluorination results in the elongation of the c axis of about 2 \AA compared to the starting oxide $\text{La}_4\text{Ni}_3\text{O}_{10}$: $P2_1/a$ $a = 5.4234 \text{ \AA}$, $b = 5.4732 \text{ \AA}$, $c = 28.0041 \text{ \AA}$, and $\beta = 90.15^\circ$ ⁵⁹ which is indicative for the insertion of F^- into the interstitial sites of the rock salt layer, and indeed a full occupation of this interstitial position is found from refining the occupation of this position. Additionally, an increase of b and therefore of the distortion of the basal ab -plane is observed, which is accompanied by an increase in the monoclinic angle β . Both observations are the result of an increased tilting distortion of the $\text{Ni}(\text{O},\text{F})_6$ octahedra



compared to the starting oxide. This is different to the structure of $\text{La}_4\text{Co}_3\text{O}_{10}\text{F}_2$, where the fluorination results in a stronger elongation of c ($\sim 3 \text{ \AA}$) that is accompanied by a decrease of the ab -distortion, a β value close to 90° and smaller tilting components of the perovskite octahedra.³⁸ Such different structural behavior upon fluorination is in line with the results obtained for the $n = 1$ oxyfluorides of nickel and cobalt. Here the Co-oxyfluoride shows a similar strong elongation of c ($\sim 2.6 \text{ \AA}$) and a decrease of the ab -distortion.²⁷ For the Ni-oxyfluorides $\text{La}_2\text{NiO}_3\text{F}_2$ and $\text{La}_2\text{NiO}_{2.5}\text{F}_3$ on the other hand, less pronounced elongations in c are accompanied by strong changes in ab and a significant increase of the octahedra tilting even though no full interlayer occupation was found for the Ni-oxyfluorides.^{19,46} In the refinements the site occupation factors were fixed to unity after preliminary tests due to the limited quality of the present data. Attempts to refine the anionic occupation factors or the isotropic thermal displacement parameters resulted in unrealistic values due to highly correlated parameters and the strong anisotropic reflection broadening. The difference Fourier map obtained for the NPD data gave no hints for partial anion occupation. Therefore, SOF values were used for all anion positions which is in concordance with the results of the chemical analysis. As the almost identical scattering lengths of O and F do not allow a clear assignment of the remaining 1.5 F^- to specific positions, we performed additional bond valence sum analysis (BVS) for selected anion distributions (results are shown in Table S 1). All models in which the terminal apical O/F(6) site is solely occupied by F^- gave a significantly reduced global instability index (GII) of $\sim 8\%$ compared to statistical distribution (GII: $\sim 11\%$). The tested model with the lowest global instability index (GII (7.7 %) involves full occupation of the O/F(6) site by F^- and an occupation of one quarter of each of the central equatorial anion sites (O/F(9) and O/F(10)). This distribution is unusual, as occupation of the equatorial sites has never been observed in other RP oxyfluorides. Another model takes the short atomic distance of Ni(4)-O/F(5) into account and comes with a full occupation of the O/F(6) site by F^- , full occupation of O/F(5) by O^{2-} and a statistical distribution of the remaining F^- over the other octahedral anion sites. The



GII of this model (7.9 %) is nearly as good as the one mentioned above. It is therefore very likely for the O/F(6) site to be occupied only by F⁻, whereas a clear statement about the distribution of the remaining 0.5 F⁻/f.u. is not unambiguously possible. We therefore opted for a statistical distribution of the remaining F⁻ to the remaining anion positions (please note that the atoms of these positions are shown as oxygen in Figure 5). To obtain charge neutrality, nickel has to partly to be in oxidation state +2. The Ni(4) site has the lowest BVS, we therefore choose an 0.5:0.5 occupation of this site by Ni³⁺ and Ni²⁺.”

Table 1: Structural parameters of La₄Ni₃O_{8.4}F_{3.5} obtained from joint Rietveld refinements of XRD, and ND data.^a

Atom	Anion Site	<i>x/a</i>	<i>y/b</i>	<i>z/c</i>	<i>U</i> _{iso} [Å ²]	Occ.	Wyck.
La(1)		0.4945(2)	0.5037(13)	0.4343(19)	0.0160	1	4 <i>e</i>
La(2)		0.0087(7)	0.4969(18)	0.0667(2)	0.0160	1	4 <i>e</i>
La(3)		0.0786(2)	1.0019(16)	0.3117(3)	0.0160	1	4 <i>e</i>
La(4)		0.5015(2)	1.0032(17)	0.1942(3)	0.0160	1	4 <i>e</i>
Ni(1)		1/2	0	1/2	0.0073	1	2 <i>b</i>
Ni(2)		0	0	0	0.0073	1	2 <i>a</i>
Ni(3)		0.0050(3)	0.5030(3)	0.3705(3)	0.0073	1	4 <i>e</i>
Ni(4)		0.0085(3)	0.9966(3)	0.1236(4)	0.0073	1	4 <i>e</i>
O/F(1)	<i>te</i>	0.2568(10)	0.2419(6)	0.1422(17)	0.0167	1	4 <i>e</i>
O/F(2)	<i>te</i>	0.2804(9)	0.7115(6)	0.3638(14)	0.0167	1	4 <i>e</i>
O/F(3)	<i>te</i>	0.2524(7)	0.7426(5)	0.6227(15)	0.0051	1	4 <i>e</i>
O/F(4)	<i>te</i>	0.2629(9)	0.7562(6)	0.1195(16)	0.0167	1	4 <i>e</i>
O/F(5)	<i>ta</i>	-0.0022(8)	0.4765(7)	0.3146(11)	0.0167	1	4 <i>e</i>
O/F(6)	<i>ta</i>	0.0278(8)	0.9468(7)	0.1930(12)	0.0167	1	4 <i>e</i>
O/F(7)	<i>ca</i>	0.4892(9)	0.9489(8)	0.4345(13)	0.0167	1	4 <i>e</i>
O/F(8)	<i>ca</i>	0.5026(7)	0.4400(7)	0.0611(13)	0.0167	1	4 <i>e</i>
O/F(9)	<i>ce</i>	0.2121(9)	0.7835(7)	0.5025(11)	0.0167	1	4 <i>e</i>
O/F(10)	<i>ce</i>	0.2525(7)	0.7521(7)	0.0102(12)	0.0167	1	4 <i>e</i>
F(1)	<i>i</i>	0.2535(9)	0.2297(5)	0.2512(13)	0.0105	1	4 <i>e</i>
F(2)	<i>i</i>	0.2143(11)	0.7253(5)	0.2595(12)	0.0105	1	4 <i>e</i>

space group: ***P2₁/a*** (14)

$R_w = 5.44\%$, $\chi^2 = 1.33$, GOF = 1.15

$a = 5.4206(3)$ Å, $b = 5.5081(3)$ Å, $c = 29.9823(18)$ Å

$\alpha = \gamma = 90^\circ$, $\beta = 90.85(4)^\circ$

$V = 895.10(6)$ Å³

^aOctahedral anion sites have a 85%/15% oxide/fluoride occupation. The sum formula is taken as La₄Ni₃O_{8.5}F_{3.5}.



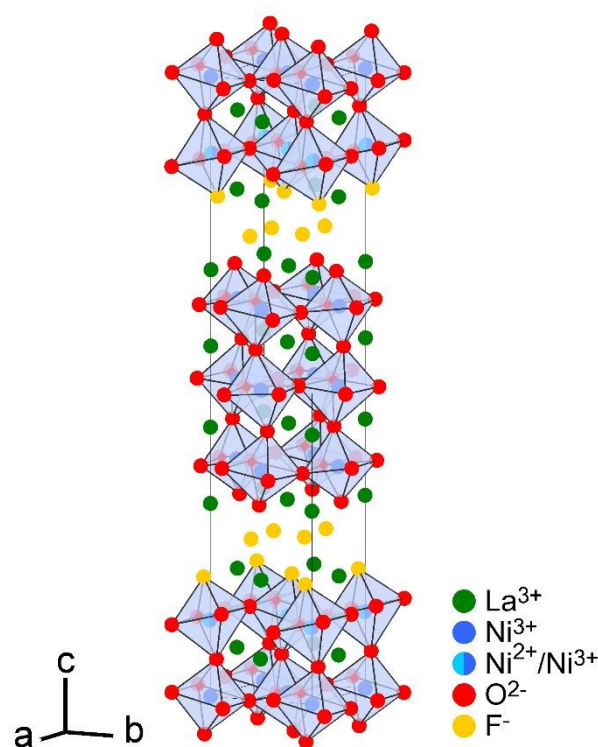


Figure 5: Crystal structure of $\text{La}_4\text{Ni}_3\text{O}_{8.4}\text{F}_{3.5}$ (space group $P2_1/a$) with representation of Ni-coordination polyhedra.

The structure derived from the Rietveld refinements is shown in Figure 5 and the atomic distances and angles are reported in the SI (Table S 2 and Table S 3). A strong tilting of the octahedra is apparent and additionally all four different octahedra are clearly distorted. This is especially true for the terminal octahedra, which include three different anion positions. The terminal apical anion position deviates in a way that this position seems to not follow the overall tilt of the octahedra (compare Figure 5 and S 10). Interestingly, similarly strong distorted octahedra were published for $\text{La}_4\text{Ni}_3\text{O}_{10}$, and $\text{La}_4\text{CoO}_{10}\text{F}_2$ especially showing the deflection of the terminal apical anion position.^{38,59} On the other hand, the anion positions are subject to an increased uncertainty due to the strong reflection broadening in combination with the complexity of the structure and the resulting high number of refinable variables. For a more precise structural description less anisotropic broadened diffraction data would be needed. Alternatively, modeling of the stacking faults with the FAUTLS/DIFFaX^{60,61} program might enable a better refinement of the diffraction data.



Thermal stability

View Article Online
DOI: 10.1039/D5DT01138H

To investigate the thermal stability of the oxyfluoride, temperature dependent XRD measurements up to 900 °C were performed on a laboratory diffractometer in dynamic gas atmosphere (40 mL/min) N₂, air, and O₂ using a homemade ‘Norby like’ capillary reactor,⁶² which was modified in order to position the transfer capillary of a mass spectrometer close to the surface sample (see Figure S 1 for a sketch and a photograph). With this setup we were able to analyze the evolving gases, gaining a deeper knowledge of such reactions. The thermal evolution of the diffraction patterns in the region of the most intense peaks are shown as contour plots in Figure 6. The decomposition proceeds via a reaction intermediate, which is clearly visible from additional peaks in the temperature region 500 to 600 °C in all 3 contour plots. From the *in situ* MS data obtained in N₂ atmosphere (compare Figure S 11) a release of oxygen was found to be linked with the formation of this intermediate decomposition product. The

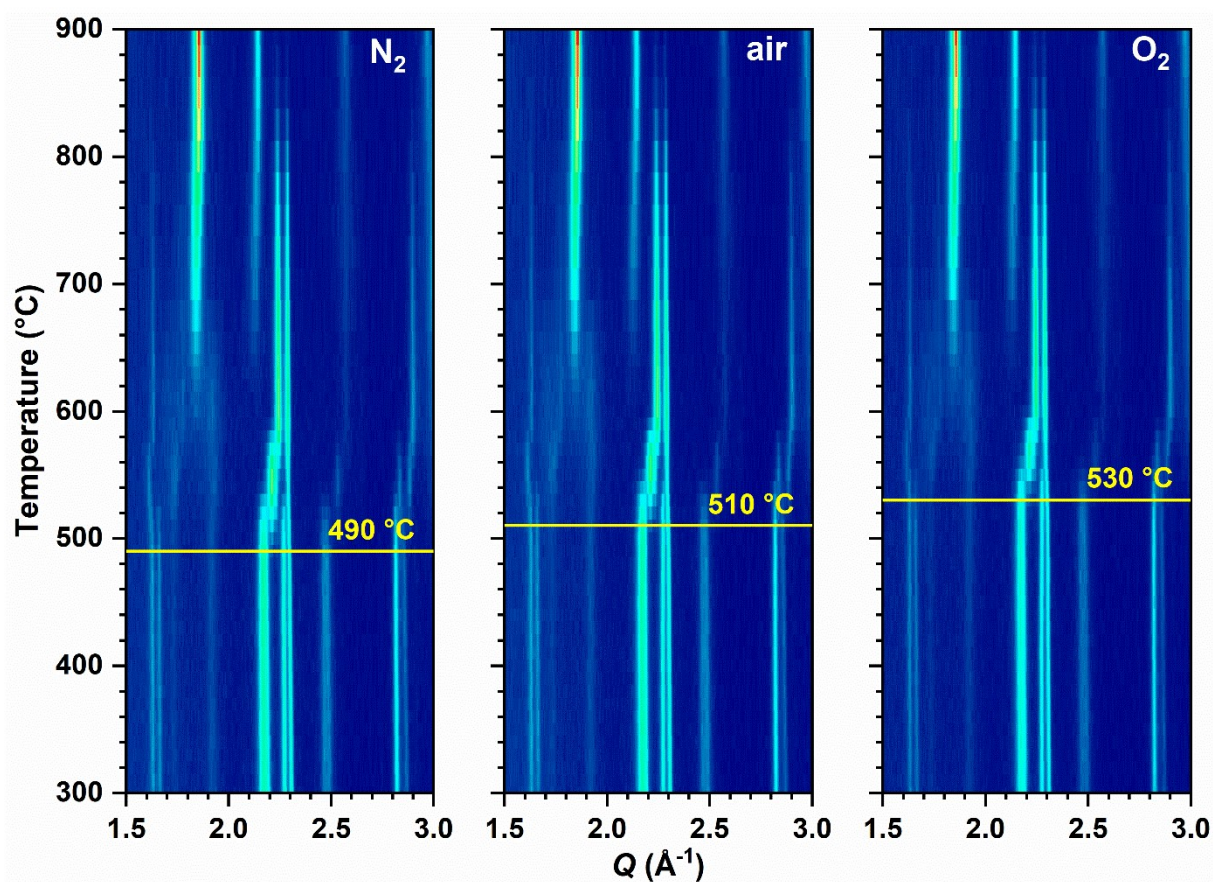


Figure 6: Contour plots of the *in situ* XRD patterns obtained for the thermal decomposition of La₄Ni₃O_{8.4}F_{3.5} in different atmospheres. The start of the decomposition is highlighted by a yellow line in each plot.



oxygen release was also observed in additional thermogravimetric experiments indicating that ~ 0.5 O per formula unit is released in this first step (as shown in the supplement Figure S 12). The formation of the decomposition intermediate is therefore linked to a partial reduction of Ni^{3+} to Ni^{2+} while the full reduction of all Ni^{3+} atoms to Ni^{2+} would result in the release of ~ 1.25 O per formula unit. The reaction is clearly linked to the oxygen partial pressure in the reaction atmosphere, which leads to different onset temperatures (defined as the temperature step where first signals of the next phase are observable) for the different reaction atmospheres. For the heating in N_2 an onset temperature of 490°C is obtained, which increases to 510°C in air and 530°C in O_2 . It is noteworthy that the decomposition intermediate observed here is not the same as the one found in the fluorination reaction (see Figure 2). The decomposition intermediate has a smaller unit cell than $\text{La}_4\text{Ni}_3\text{O}_{8.4}\text{F}_{3.5}$, reflected by the significant shift in the main reflections towards higher Q values. With increasing temperature, the oxyfluoride further releases oxygen (see the TG-MS results Figure S 12) and the reflections of an $n = 3$ RP-phase similar to the starting oxide are observed. In all cases LaOF and NiO were identified as the decomposition products above 650°C as is often observed upon decomposition of La containing RP oxyfluorides.^{19,46} When performing the *in situ* XRD-MS experiment in a reducing atmosphere (10% H_2 in N_2 , compare Figure S13) LaOF is observed as decomposition product, while signals of Ni(0) are not found. This is most probably the result of a weak amorphous contribution to the diffraction pattern which is in contrast to the hard character of the Mo radiation used (please note that even the amorphous contribution of the glass capillary is missing from the diffraction data). From this experiment it is additionally found that the reductive decomposition of $\text{La}_4\text{Ni}_3\text{O}_{8.4}\text{F}_{3.5}$ proceeds via at least two intermediates which were not further investigated yet but clearly differ from the above observed decomposition intermediates. Such partially reduced oxyfluorides are of high interest and attempts to isolate them will be pursued in future studies. The thermal stability of the title compound is comparable to the $n = 1$ nickel-based oxyfluoride $\text{La}_2\text{NiO}_3\text{F}_2$ ($\sim 450^\circ\text{C}$), while the higher fluorinated

View Article Online
DOI: 10.1039/D5DT01138H

Dalton Transactions Accepted Manuscript



compound $\text{La}_2\text{NiO}_{2.5}\text{F}_3$ exhibits a significantly lower thermal decomposition temperature ($\sim 380^\circ\text{C}$).^{19,40,46,47}

View Article Online
DOI: 10.1039/D5DT01138H

Magnetic Properties

The precursor oxide $\text{La}_4\text{Ni}_3\text{O}_{10}$ has previously been reported to be a Pauli paramagnet as the result of electron exchange between nickel sites with two different oxidation states (Ni^{2+} , and Ni^{3+}). A weak susceptibility minimum around 90 K is additionally linked to a metal-to-metal transition.^{63,64} This magnetic behaviour was also found for the precursor oxide of this study for which the χ_{mol} vs. T data is shown in Figure 7a. Upon fluorination a strong impact on the exchange interactions between different perovskite slabs is expected and was previously observed for $\text{La}_4\text{Co}_3\text{O}_{10}\text{F}_2$,³⁸ and nickelate oxyfluorides with $n = 2$, and 1.^{35,46,47} The results of the temperature dependent susceptibility measurements for $\text{La}_4\text{Ni}_3\text{O}_{8.4}\text{F}_{3.5}$ in an external field

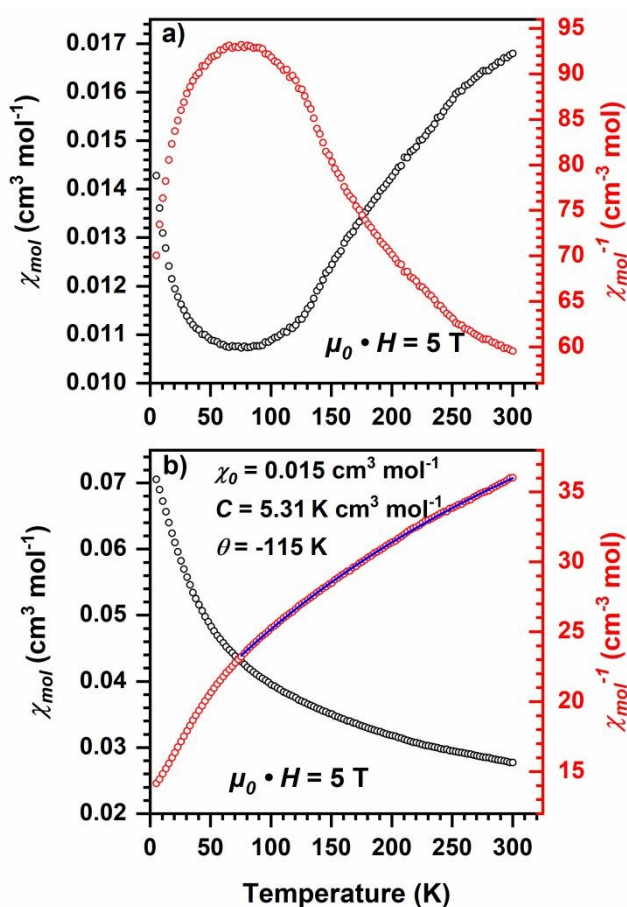


Figure 7: Temperature dependent susceptibility (black) and inverse susceptibility (red) data of a) $\text{La}_4\text{Ni}_3\text{O}_{10}$ and b) $\text{La}_4\text{Ni}_3\text{O}_{8.4}\text{F}_{3.5}$ at 5 T. For the oxyfluoride the inverse susceptibility was fitted using an extended Curie-Weiss law (blue line) in the range of 75 K to 300 K.



of 5 T are shown in Figure 7b) and reflects a Curie-Weiss behavior. As the inverse susceptibility shows a clear curvature the data was fitted with an extended Curie-Weiss law $\frac{1}{\chi_{mol}} = \frac{1}{\frac{C}{T-\theta} + \chi_0}$ compromising a temperature independent contribution (χ_0). The fit is shown in Figure 7b and the obtained Curie constant of $5.31 \text{ cm}^3 \text{ K mol}^{-1}$ corresponds to a paramagnetic moment of $\mu_{\text{eff}} = 1.84 \mu_{\text{B}}$. This is in fairly good agreement with the value of $2.04 \mu_{\text{B}}$ expected for Ni with an observed average oxidation state of 2.76 and Ni^{3+} being in a low-spin configuration. If Ni^{3+} is considered to be in high-spin configuration, the expected moment is $3.65 \mu_{\text{B}}$, which is much larger than the observed value. However, it should be kept in mind that the Curie-Weiss law in principle only applies to isolated ions which is why such values should not be overinterpreted. Furthermore, the value of C , and in turn of μ_{eff} , is highly dependent on the temperature interval used for the fit. The Weiss temperature of $\theta \approx -115 \text{ K}$ is indicative of antiferromagnetic interactions but no clear sign of a long-range magnetic ordering was observed neither in the 5 T nor in the 0.1 T data (see Figure S 14). Our investigations show that fluorination strongly alters the magnetic properties compared to the parent oxide most probably due the partially oxidation of Ni^{2+} to Ni^{3+} resulting in less delocalized electrons.

Conclusions

The Ruddlesden-Popper oxyfluoride $\text{La}_4\text{Ni}_3\text{O}_{8.4}\text{F}_{3.5}$ with a mixed $\text{Ni}^{2+/3+}$ oxidation state was prepared for the first time by topochemical fluorination of a $\text{La}_4\text{Ni}_3\text{O}_{10}$ precursor from the citrate synthesis with PVDF as fluorine source. The chemical composition of this compound was confirmed by several analytical methods. $\text{La}_4\text{Ni}_3\text{O}_{8.4}\text{F}_{3.5}$ crystallizes in the same space group as the parent oxide $P2_1/a$ and the presence of strongly anisotropic broadened (hkl) reflections with $l \neq 0$ points to stacking faults related to the thickness of the perovskite layers. $\text{La}_4\text{Ni}_3\text{O}_{8.4}\text{F}_{3.5}$ is stable up to 510°C in air (490°C in N_2 and 530°C in O_2) and the thermal decomposition is accompanied by release of oxygen as found by XRD-MS and TG-MS measurements. $\text{La}_4\text{Ni}_3\text{O}_{8.4}\text{F}_{3.5}$ is a Curie-Weiss magnet with a Weiss constant of $\theta \approx -115 \text{ K}$,



indicating antiferromagnetic interactions. The observed paramagnetic magnetic moment of

[View Article Online](#)
DOI: 10.1039/D5DT01138H

$\mu_{\text{eff}} = 1.84 \mu_{\text{B}}$ points to low-spin configuration of Ni^{3+} .



Author Contributions

View Article Online
DOI: 10.1039/D5DT01138H

J.G conceptualization, formal analysis, investigation, methodology, visualization, writing – original draft **S.G.E.:** supervision, resources, writing - review & editing **J.J.:** supervision, conceptualization, data curation, investigation, formal analysis, visualization, writing – review & editing

Conflicts of interest

The authors declare that they have no known competing financial interests or personal relationships that could have appeared to influence the work reported in this paper.

Data availability

The data supporting the findings of this study are available within the article and its ESI. The crystallographic data of $\text{La}_4\text{Ni}_3\text{O}_{8.4}\text{F}_{3.5}$ has been deposited at the CCDC under deposition number 2451197, and can be obtained from <https://www.ccdc.cam.ac.uk/>. The neutron diffraction data is available under the following link <https://doi.ill.fr/10.5291/ILL-DATA.5-23-769>. Any other information should be requested to the corresponding authors.

Acknowledgements

The neutron diffraction experiment was performed on the D2B diffractometer run by the Institut Laue-Langevin (ILL); beamtime was granted under the proposal number 5-23-769.⁴⁸ We thank Dr. Clemens Ritter for performing the measurement, and we thank the ILL for the allocated beamtime. We thank Eik Koslowski for performing the XPS measurements.



References

- 1 S. Liu, M. Avdeev, Y. Liu, M. R. Johnson and C. D. Ling, *Inorg. Chem.*, 2016, **55**, 1403–1411.
- 2 Z. Li, W. Guo, T. T. Zhang, J. H. Song, T. Y. Gao, Z. B. Gu and Y. F. Nie, *APL Mater.*, 2020, **8**, 091112.
- 3 A. Bivour, J. Jacobs, F. Daumann, G. Hörner, B. Weber, C. Ritter and S. G. Ebbinghaus, *Inorg. Chem.*, 2024, **63**, 20427–20437.
- 4 X. Sun, Y. Mi, F. Jiao and X. Xu, *ACS Catal.*, 2018, **8**, 3209–3221.
- 5 G. Gou, M. Zhao, J. Shi, J. K. Harada and J. M. Rondinelli, *Chem. Mater.*, 2020, **32**, 2815–2823.
- 6 T. Nagai, H. Shirakuni, A. Nakano, H. Sawa, H. Moriwake, I. Terasaki and H. Taniguchi, *Chem. Mater.*, 2019, **31**, 6257–6261.
- 7 K.-E. Hasin, N. Pokhrel and E. A. Nowadnick, *Chem. Mater.*, 2024, **36**, 7552–7560.
- 8 H. Yaguchi, K. Fujii, Y. Tsuchiya, H. Ogino, Y. Tsujimoto and M. Yashima, *ACS Appl. Energy Mater.*, 2022, **5**, 295–304.
- 9 N. A. Tarasova, *Chim. Tech. Acta*, 2022, **9**, 20229415.
- 10 J. W. González, A. M. León, C. González-Fuentes and R. A. Gallardo, *Nanoscale*, 2025, **17**, 4796–4807.
- 11 F. Bernardini, M. Fiebig and A. Cano, *J. Appl. Phys.*, 2025, **137**, 103903.
- 12 C. Park and R. L. Snyder, *Appl. Supercond.*, 1995, **3**, 73–83.
- 13 H. Sun, M. Huo, X. Hu, J. Li, Z. Liu, Y. Han, L. Tang, Z. Mao, P. Yang, B. Wang, J. Cheng, D.-X. Yao, G.-M. Zhang and M. Wang, *Nature*, 2023, **621**, 493–498.
- 14 O. J. Hernandez, G. Geneste, T. Yajima, Y. Kobayashi, M. Okura, K. Aidzu, C. Tassel, S. Paofai, D. Swain, C. Ritter and H. Kageyama, *Inorg. Chem.*, 2018, **57**, 11058–11067.
- 15 H. Sonoki, Daisuke Mori, S. Taminato, Y. Takeda, O. Yamamoto and N. Imanishi, *Chem. Commun.*, 2019, **55**, 7454–7457.
- 16 Y. Bréard, B. Raveau, D. Pelloquin and A. Maignan, *J. Mater. Chem.*, 2007, **17**, 2818–2823.
- 17 D. Pelloquin, N. Barrier, D. Flahaut, V. Caignaert and A. Maignan, *Chem. Mater.*, 2005, **17**, 773–780.
- 18 O. Clemens and P. R. Slater, *Rev. Inorg. Chem.*, 2013, **33**, 105–117.
- 19 J. Jacobs, M. A. L. Marques, H.-C. Wang, E. Dieterich and S. G. Ebbinghaus, *Inorg. Chem.*, 2021, **60**, 13646–13657.
- 20 C. S. Knee and M. T. Weller, *Chem. Commun.*, 2002, 256–257.
- 21 A. L. Hector, J. A. Hutchings, R. L. Needs, M. F. Thomas and M. T. Weller, *J. Mater. Chem.*, 2001, **11**, 527–532.
- 22 Y. Bréard, C. Michel, M. Hervieu and B. Raveau, *J. Mater. Chem.*, 2000, **10**, 1043–1045.
- 23 E. E. McCabe and C. Greaves, *J. Fluor. Chem.*, 2007, **128**, 448–458.
- 24 F. Galasso and W. Darby, *J. Phys. Chem.*, 1962, **66**, 1318–1320.
- 25 L.-S. Du, F. Wang and C. P. Grey, *J. Solid State Chem.*, 1998, **140**, 285–294.
- 26 G. S. Case, A. L. Hector, W. Levason, R. L. Needs, M. F. Thomas and M. T. Weller, *J. Mater. Chem.*, 1999, **9**, 2821–2827.
- 27 M. A. Nowroozi, S. Ivlev, J. Rohrer and O. Clemens, *J. Mater. Chem. A*, 2018, **6**, 4658–4669.
- 28 L. D. Aikens, L. J. Gillie, R. Li and C. Greaves, *J. Mater. Chem.*, 2002, **12**, 264–267.
- 29 T. Baikie, E. L. Dixon, J. F. Rooms, N. A. Young and M. G. Francesconi, *Chem. Commun.*, 2003, 1580–1581.
- 30 P. R. Slater and R. K. B. Gover, *J. Mater. Chem.*, 2002, **12**, 291–294.
- 31 T. Sivakumar and J. B. Wiley, *Materials Research Bulletin*, 2009, **44**, 74–77.
- 32 R. Zhang, G. Read, F. Lang, T. Lancaster, S. J. Blundell and M. A. Hayward, *Inorg. Chem.*, 2016, **55**, 3169–3174.
- 33 Y. Tsujimoto, K. Yamaura, N. Hayashi, K. Kodama, N. Igawa, Y. Matsushita, Y. Katsuya, Y. Shirako, M. Akaogi and E. Takayama-Muromachi, *Chem. Mater.*, 2011, **23**, 3652–3658.
- 34 R. L. Needs and M. T. Weller, *J. Chem. Soc., Dalton Trans.*, 1995, 3015–3017.
- 35 R. Zhang, M. S. Senn and M. A. Hayward, *Chem. Mater.*, 2016, **28**, 8399–8406.



- 36 K. Wissel, T. Vogel, S. Dasgupta, A. D. Fortes, P. R. Slater and O. Clemens, *Inorg. Chem.*, 2020, **59**, 1153–1163. Article Online
DOI: 10.1039/D5DT01138H
- 37 N. N. M. Gurusinge, J. C. Fones, J. F. Marco, F. J. Berry and C. Greaves, *Dalton Trans.*, 2014, **43**, 2038–2043.
- 38 B. Gonano, Ø. S. Fjellvåg, G. Steciuk, K. Marshall, H. Fjellvåg and M. Valldor, *Scr. Mater.*, 2025, **255**, 116379.
- 39 C. K. Blakely, S. R. Bruno, S. K. Kraemer, A. M. Abakumov and V. V. Poltavets, *J. Solid State Chem.*, 2020, **289**, 121490.
- 40 P. R. Slater, *J. Fluor. Chem.*, 2002, **117**, 43–45.
- 41 P. R. Slater, P. P. Edwards, C. Greaves, I. Gameson, M. G. Francesconi, J. P. Hodges, M. Al-Mamouri and M. Slaski, *Phys. C: Supercond.*, 1995, **241**, 151–157.
- 42 C. Greaves, J. L. Kissick, M. G. Francesconi, L. D. Aikens and L. J. Gillie, *J. Mater. Chem.*, 1999, **9**, 111–116.
- 43 P. R. Slater, J. P. Hodges, M. G. Francesconi, C. Greaves and M. Slaski, *J. Mater. Chem.*, 1997, **7**, 2077–2083.
- 44 G. B. Peacock, I. Gameson, M. Slaski, J. J. Capponi and P. P. Edwards, *Phys. C: Supercond. Appl.*, 1997, **289**, 153–160.
- 45 M. Al-Mamouri, P. P. Edwards, C. Greaves, P. R. Slater and M. Slaski, *J. Mater. Chem.*, 1995, **5**, 913.
- 46 K. Wissel, J. Heldt, P. B. Groszewicz, S. Dasgupta, H. Breitzke, M. Donzelli, A. I. Waidha, A. D. Fortes, J. Rohrer, P. R. Slater, G. Buntkowsky and O. Clemens, *Inorg. Chem.*, 2018, **57**, 6549–6560.
- 47 J. Jacobs, H.-C. Wang, M. A. L. Marques, K. Xu, J. Schmedt Auf Der Günne and S. G. Ebbinghaus, *Inorg. Chem.*, 2024, **63**, 6075–6081.
- 48 S. G. Ebbinghaus, A. Bivour, J. Jacobs and C. Ritter, DOI:10.5291/ILL-DATA.5-23-769.
- 49 B. H. Toby and R. B. Von Dreele, *J. Appl. Crystallogr.*, 2013, **46**, 544–549.
- 50 J. Jacobs, A. Bivour, V. Sikolenko, H. Kohlmann, T. C. Hansen, J. R. Hester, K. Xu, J. Schmedt Auf Der Günne and S. G. Ebbinghaus, *J. Am. Chem. Soc.*, 2025, **147**, 9739–9751.
- 51 R. Clauberg, W. Gudat, E. Kisker, E. Kuhlmann and G. M. Rothberg, *Phys. Rev. Lett.*, 1981, **47**, 1314–1317.
- 52 J. F. Moulder, W. F. Stickle, P. E. Sobol and K. D. Bomben, *Handbook of X-ray Photoelectron Spectroscopy: A Reference Book of Standard Spectra for Identification and Interpretation of XPS Data*, ed. J. Chastain, Perkin-Elmer Corporation, Physical Electronics Division, Eden Prairie, MN, 1992.
- 53 X. Ning, Z. Wang and Z. Zhang, *Sci Rep*, 2015, **5**, 8460.
- 54 A. Jarvis, F. J. Berry, J. F. Marco, M. Sanchez-Arenillas, G. Cibin, O. Clemens and P. R. Slater, *J. Solid State Chem.*, 2020, **287**, 121372.
- 55 R. Seshadri, M. Hervieu, C. Martin, A. Maignan, B. Domenges, B. Raveau and A. N. Fitch, *Chem. Mater.*, 1997, **9**, 1778–1787.
- 56 M. Periyasamy, L. Patra, Ø. S. Fjellvåg, P. Ravindran, M. H. Sørby, S. Kumar, A. O. Sjøstad and H. Fjellvåg, *ACS Appl. Electron. Mater.*, 2021, **3**, 2671–2684.
- 57 A. S. Gorkusha, S. V. Cherepanova and S. V. Tsybulya, *J. Appl. Crystallogr.*, 2024, **57**, 1578–1587.
- 58 P. W. Stephens, *J Appl Crystallogr*, 1999, **32**, 281–289.
- 59 S. Kumar, Ø. Fjellvåg, A. O. Sjøstad and H. Fjellvåg, *J. Magn. Magn. Mater.*, 2020, **496**, 165915.
- 60 M. Casas-Cabanas, J. Rodríguez-Carvajal, J. Canales-Vázquez, Y. Laligant, P. Lacorre and M. R. Palacín, *J. Power Sources*, 2007, **174**, 414–420.
- 61 M. M. J. Treacy, J. M. Newsam and M. W. Deem, *Proc. R. Soc. Lond. A*, 1991, **433**, 499–520.
- 62 P. Norby, *J. Am. Chem. Soc.*, 1997, **119**, 5215–5221.
- 63 M. U. Nagell, S. Kumar, M. H. Sørby, H. Fjellvåg and A. O. Sjøstad, *Ph. Transit.*, 2015, **88**, 979–990.
- 64 M. D. Carvalho, M. M. Cruz, A. Wattiaux, J. M. Bassat, F. M. A. Costa and M. Godinho, *J. Appl. Phys.*, 2000, **88**, 544–549.



The data supporting the findings of this study are available within the article and its ESI. The crystallographic data of $\text{La}_4\text{Ni}_3\text{O}_{8.4}\text{F}_{3.5}$ has been deposited at the CCDC under deposition number 2451197, and can be obtained from <https://www.ccdc.cam.ac.uk/>. The neutron diffraction data is available under the following link <https://doi.ill.fr/10.5291/ILL-DATA.5-23-769>. Any other information should be requested to the corresponding authors.

